Studies of Silicoaluminophosphates with the Sodalite Structure

Dennis Hasha,[†] Ligia Sierra de Saldarriaga,[‡] Carlos Saldarriaga,[‡] Paul E. Hathaway,[§] David F. Cox,[§] and Mark E. Davis*[§]

Contribution from the Department of Chemical Engineering, Virginia Polytechnic Institute and State University, Blacksburg, Virginia 24061, and The Analytical Laboratory, The Dow Chemical Company, Midland, Michigan 48640. *Received August 6, 1987*

Abstract: The tetrahedral atom arrangements of silicon, phosphorus, and aluminum in silicoaluminophosphates with sodalite structure have been elucidated. No evidence of Si-O-P linkages is provided. Silicon atoms are found to have silicon and/or aluminum neighbors while phosphorus is surrounded by aluminum only. Two distinct physicochemical environments of aluminum are observed: phosphorus rich and silicon rich.

New crystalline, microporous molecular sieves have been reported recently.[1] These novel materials are aluminophosphate molecular sieves that have been incorporated with other elements. To date, 13 elements have been employed.[1] The catalytic properties of several silicoaluminophosphates[1-7] (SAPO-*n*)[8] and other substituted aluminophosphates[1,7,9] show that these materials exhibit unique conversion abilities for a broad spectrum of hydrocarbon reactions.

These new solids consist of tetrahedral oxide frameworks. For example, the SAPO molecular sieves contain oxide tetrahedra of silicon, aluminum, and phosphorus arranged in a manner that can be considered as silicon substitution into a hypothetical $AlPO_4$-*n* framework. The silicon substitution can be for (1) aluminum, (2) phosphorus, or (3) an aluminum-phosphorus pair.[4b] Similar substitutions with other elements are postulated to occur in the formation of MeAPO, MeAPSO, ElAPO, and ElAPSO[1] materials. Lok et al.[4b] report that mechanisms 2 and 3 are more likely than mechanism 1 for the SAPO materials since they exhibit cation exchange and they show an excess of aluminum over phosphorus.

We have been investigating the tetrahedral atom arrangements in substituted, aluminophosphate molecular sieves and have reported recently on SAPO-37.[10] SAPO-37 is the silicoaluminophosphate with the structure of faujasite. This molecular sieve framework contains a homogeneous distribution of silicon, aluminum, and phosphorus and is negatively charged. We conclusively showed that silicon substitutes into the hypothetical aluminophosphate framework by mechanism 2 alone. Previous work on SAPO-*n* molecular sieves[11,12] other than SAPO-37 provides speculative evidence for mechanisms 2 and/or 3. Thus, in order to generalize our conclusions from SAPO-37 to the complete category of SAPO-*n* molecular sieves, we expanded our investigation to include a series of SAPO's in which the framework structure is maintained constant while the composition of Si, Al, and P tetrahedral atoms is varied.

The purpose of our work is to investigate the nature of silicon substitution into hypothetical aluminophosphate frameworks. We synthesized five molecular sieves with framework compositions spanning the range from aluminophosphate through the SAPO region to sodalite (aluminosilicate). All five materials possess the same framework structure, that being the sodalite structure.[13] Complete study of these materials allows us to overcome the limitations in generalizing our previous conclusions for SAPO-37[10] to the entire category of SAPO-*n* materials.

Experimental Section

a. Samples. The molecular sieves SAPO-20A, SAPO-20B, and SAPO-20C were synthesized according to the procedure outlined in the Union Carbide patent.[4a] We were not able to crystallize pure $AlPO_4$-20 using the procedure of the Union Carbide patent.[14] However, we were able to synthesize pure $AlPO_4$-20 using the following method. Solution 1 was prepared by adding 3.5 g of 85 wt % H_3PO_4 to 5.5 g of H_2O. Next, 2.1 g of pseudo boehmite alumina (Catapal-B) was added to solution 1 with stirring. Solution 2 was prepared by adding 3.8 g of 40 wt % tetrapropylammonium hydroxide ((TPA)OH) and 1.4 g of tetramethylammonium hydroxide pentahydrate ((TMA)OH·$5H_2O$) to 3.0 g of H_2O. Solution 2 was added to solution 1 with mixing and then aged at 0 °C for 2 days. The gel was heated to 200 °C at autogenous pressure for 16 h. Sodalite was synthesized by the following method. The gel was prepared by adding 9.9 g of (TMA)OH·$5H_2O$ to 13.6 g of H_2O. Next, 4.6 g of fumed silica (Cab-O-Sil) was added to the solution with stirring. Finally, 1.0 g of pseudo boehmite alumina and 5.1 g of H_2O were added with good agitation. The gel was aged at room temperature for 5 days after which it was heated to 200 °C at autogenous pressure for 4 days. A summary of the synthesis gel compositions used in this study is given in Table I. Notice that, for all preparations other than for SAPO-20C, no alkali cations are added to the gels.

b. Analysis. Magic angle spinning ^{13}C, ^{29}Si, ^{27}Al, and ^{31}P NMR spectra were recorded on a Bruker CXP 200 spectrometer. The ^{13}C spectra were obtained at a frequency of 50.3 MHz and a rotation rate of 3-4 kHz. Chemical shifts are reported relative to Me_4Si but were referenced to hexamethylbenzene (16.9 ppm relative to Me_4Si), which was used as an internal standard. Resolution enhancement of the SAPO-20A FID was accomplished by standard mathematical procedures (vide infra). The ^{29}Si spectra were taken at a frequency of 39.7 MHz and a spinning frequency of 3-4 kHz. Chemical shifts are reported relative to Me_4Si. Magic angle spinning ^{27}Al spectra were recorded at 52.15 MHz and a rotation rate of 3-5 kHz. The ^{27}Al chemical shifts are reported relative to $Al(NO_3)_3$ in aqueous solution at infinite dilution and are not corrected for second-order quadrupole effects. The ^{31}P spectra were taken at a frequency of 81.0 MHz and a spinning rate of 4.5-5 kHz. Chemical shifts are reported relative to 85 wt % H_3PO_4.

Thermogravimetric analyses (TGA) and differential thermal analysis (DTA) were performed in air on a Du Pont 950 thermogravimetric

[†] The Dow Chemical Co.
[‡] Present address: Universidad de Antioquia, Medellin, Colombia.
[§] Virginia Polytechnic Institute and State University.

(1) Flanigen, E. M.; Lok, B. M.; Patton, R. L.; Wilson, S. T. *New Developments in Zeolite Science and Technology*; Murakami, S., Iijima, A., Ward, J. W., Eds.; Elsevier: Amsterdam, 1986; p 103 (and references therein).
(2) Qinhua, X.; Aizhen, Y.; Shulin, B.; Kaijun, X. *New Developments in Zeolite Science and Technology*; Murakami, X., Iijima, A., Ward, J. W., Eds.; Elsevier: Amsterdam, 1986; p 835.
(3) Pellet, R. J.; Long, G. N.; Rabo, J. A. *New Developments in Zeolite Science and Technology*; Murakami, X., Iijima, A., Ward, J. W., Eds.; Elsevier: Amsterdam, 1986; p 843.
(4) (a) Lok, B. M.; Messina, C. A.; Patton, R. L.; Gajek, R. T.; Cannan, T. R.; Flanigen, E. M. U.S. Patent 4440871, 1984. (b) Lok, B. M.; Messina, C. A.; Patton, R. L.; Gajek, R. T.; Cannan, T. R.; Flanigen, E. M. *J. Am. Chem. Soc.* **1984**, *106*, 6092-6093.
(5) Garska, D. C.; Lok, B. M. U.S. Patent 4499315, 1985.
(6) Kaiser, S. W. U.S. Patent 4499327, 1985.
(7) (a) Pyke, D. R.; Whitney, P.; Houghton, H. *Appl. Catal.* **1985**, *18*, 173-190. (b) Tapp, N. J.; Milestone, N. B.; Wright, L. J. *J. Chem. Soc., Chem. Commun.* **1985**, 1801-1803.
(8) The suffix "*n*" denotes a specific structure type as given in ref 4a.
(9) Kikhtyanin, O. V.; Ione, K. G.; Mastikhin, V. M. *Chem. Express* **1986**, *1*(*12*), 721-724.
(10) Sierra de Saldarriaga, L.; Saldarriaga, C.; Davis, M. E. *J. Am. Chem. Soc.* **1987**, *109*, 2686-2691.
(11) Ito, M.; Shimoyama, Y.; Saito, Y.; Tsurita, Y.; Otake, M. *Acta Crystallogr., Sect. C: Cryst. Struct. Commun.* **1985**, *C41*, 1698-1700.
(12) Appleyard, I. P.; Harris, R. K.; Fitch, F. R. *Chem. Lett.* **1985**, 1747-1750.
(13) Baerlocher, C.; Meier, W. M. *Helv. Chim. Acta* **1969**, *52*, 1853-1860.
(14) Wilson, S. T.; Lok, B. M.; Flanigen, E. M. U.S. Patent 4310440, 1982.
(15) Wilson, S. T.; Lok, B. M.; Messina, C. A.; Cannon, T. R.; Flanigen, E. M. *Intrazeolite Chemistry*; American Chemical Society: Washington, DC, 1983; pp 79-106.

0002-7863/88/1510-2127$01.50/0

Table I. Preparation Methods

sample	gel composition	procedure
$AlPO_4$-20	$0.25(TPA)_2O{\cdot}0.25(TMA)_2O{\cdot}Al_2O_3{\cdot}P_2O_5{\cdot}50H_2O$	this work
SAPO-20A	$(TMA)_2O{\cdot}1.1Al_2O_3{\cdot}1.0P_2O_5{\cdot}0.4SiO_2{\cdot}50H_2O$	Union Carbide (example 30)
SAPO-20B	$0.75(TMA)_2O{\cdot}Al_2O_3{\cdot}P_2O_5{\cdot}SiO_2{\cdot}50H_2O$	Union Carbide (example 27)
SAPO-20C	$1.1(TMA)_2O{\cdot}1.66Al_2O_3{\cdot}0.66P_2O_5{\cdot}4.0SiO_2{\cdot}2Na_2O^a{\cdot}98H_2O$	Union Carbide (example 28)
sodalite	$3.9(TMA)_2O{\cdot}Al_2O_3{\cdot}11SiO_2{\cdot}190H_2O$	this work

[a] From addition of sodium aluminate.

Table II. Chemical Compositions of Molecular Sieves

sample	oxide composition	g H_2O/g solid[a]	g organic/g solid[a]	color after TGA (to 850 °C)	approx molecules/cage[a] TMA	approx molecules/cage[a] H_2O
$AlPO_4$-20	$(Al_{0.5}P_{0.5})O_2$	0.082	0.155	light tan	0.6	1.7
$AlPO_4$-20[b]	$(Al_{0.5}P_{0.5})O_2$				1.0	
SAPO-20A	$(Al_{0.47}Si_{0.13}P_{0.40})O_2$	0.033	0.106	black	0.5	0.7
SAPO-20[c]	$(Al_{0.46}Si_{0.18}P_{0.36})O_2$					
SAPO-20B	$(Al_{0.42}Si_{0.22}P_{0.36})O_2$	0.045	0.157	gray	0.8	0.9
SAPO-20[c]	$(Al_{0.47}Si_{0.15}P_{0.38})O_2$				0.9	0.7
SAPO-20C[d]	$(Al_{0.38}Si_{0.50}P_{0.12})O_2$	0.151	0.083	gray	0.4	3.0
SAPO-20[c,d]	$(Al_{0.38}Si_{0.50}P_{0.12})O_2$				0.6	0.9
sodalite	$(Al_{0.14}Si_{0.86})O_2$	0.043	0.245	white	1.2	0.9
sodalite[e]	$(Al_{0.17}Si_{0.83})O_2$				1.0	

[a] From TGA and DTA. [b] From ref 15. [c] From ref 4a. [d] Material contains sodium. [e] From ref 13.

analyzer and 900 differential analyzer, respectively.

Infrared measurements were performed on an IBM IR/32 FTIR.

The X-ray powder diffraction pattern of all samples was recorded and indexed on a Nicolet I2 automated diffraction system. The complete powder patterns were indexed with lead nitrate as the internal standard.

Silicon, aluminum, and phoshorus were analyzed by electron microprobe analysis by using an Applied Research Laboratories SEMQ electron microprobe.

Chemical analysis of the superficial regions of the samples was performed by X-ray photoelectron spectroscopy (XPS) with a Perkin-Elmer Phi 5300 ESCA employing Mg Kα X-rays. Binding energies are referenced to the gold $4f_{7/2}$ transition at 83.8 eV (gold was sputtered onto a small spot of the sample prior to analysis).

Results and Discussion

Chemical Compositions of Molecular Sieves. The chemical compositions of the five molecular sieves used in this study are given in Table II. The chemical compositions of appropriate reference materials are provided also in Table II for comparison. The oxide composition of $AlPO_4$-20 shows the ideal 1/1 ratio of Al and P typical of aluminophosphate molecular sieves. SAPO-20 has a framework that consists of Si, Al, and P. Notice that the series SAPO-20A, SAPO-20B, and SAPO-20C show increasing relative amounts of silicon present in the oxide composition, respectively. Finally, the sodalite used here is the so-called TMA–sodalite[13] and has a silicon to aluminum ratio near 5. The measured oxide composition shows a slightly higher silicon to aluminum ratio and could be due to a small amount of amorphous silica present in the sample. Notice that these five materials span the oxide composition range from aluminophosphate through silicoaluminophosphate to aluminosilicate. Also, SAPO-20A and SAPO-20B appear to be "silicon-substituted aluminophosphates" while SAPO-20C appears to be a "phosphorus-substituted aluminosilicate". In general, our oxide compositions compare favorably to the listed reference materials. However, for SAPO-20A and SAPO-20B, our silicon contents are lower and higher, respectively, than those reported by Union Carbide. Interestingly, SAPO-20C shows the exact oxide composition as reported by Union Carbide.

The weight loss associated with water desorption and TMA combustion for the materials synthesized in our laboratory is listed also in Table II. These data are from the TGA analyses (vide infra), where specific weight losses are assigned from DTA analyses. After the samples are heated to 850 °C in the TGA chamber, the only sample that becomes white is sodalite. The color of the remaining four samples is likely due to residual carbon. Therefore, when the weight losses are converted to molecules/cage, the values listed are approximate since an unknown residue organic weight is not accounted for when the amount of TMA is calculated. Notice that sodalite shows the ideal one TMA, to within experimental error, per cage. Figure 1 illustrates the sodalite structure and shows how one TMA molecule can occupy a cage. Because of spatial constraints, only one TMA can fit in each cage. However, there is additional room for water and/or sodium along with a TMA molecule in a cage. Ideally, we expect one TMA per cage for $AlPO_4$-20 and SAPO-20. However, it is most probable that somewhere between one TMA per two cages and per one cage is the true conformation. Our data compare favorably to that of the reference materials especially since we expect our TMA/cage ratios to be low for the solids that did not become white at 850 °C. The exception to the comparison is the H_2O/cage ratio for SAPO-20C. Our material shows a significantly higher water content.

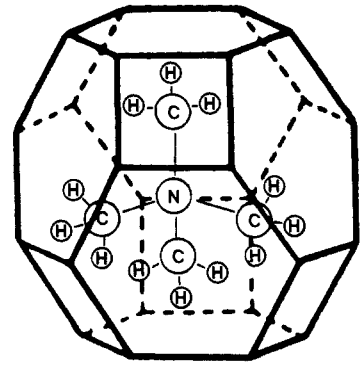

Figure 1. Model of sodalite cage with TMA molecule.

X-ray Powder Diffraction Results. X-ray powder diffraction patterns of all five materials show that they possess the sodalite structure. The structure of a sodalite cage is illustrated in Figure 1. The samples did show slight differences in d-spacings and significant variations in peak intensities. Table III gives the relative intensities for the major peaks in the X-ray powder diffraction patterns of all five materials. Notice how the relative intensities of the reflections are dependent upon the oxide composition. Relative intensity variations with oxide composition have been shown previously for substituted $AlPO_4$-5 molecular sieves.[7a] Pyke et al.[7a] report that they indexed $AlPO_4$-20 to cubic symmetry. However, we are not able to do so with our sample. Our samples showed various symmetries as the best solutions to indexing, e.g., $AlPO_4$-20 (tetragonal), SAPO-20A (orthorhombic), and SAPO-20C (cubic). Therefore, at this time further work is required prior to reporting correct unit cell information.

Table III. X-ray Powder Diffraction Data for Molecular Sieves

$AlPO_4$-20		SAPO-20A		SAPO-20B		SAPO-20C		sodalite	
d, Å	I/I_0	*d*, Å	I/I_0	*d*, Å	I/I_0	*d*, Å	I/I_0	*d*, Å	I/I_0
6.29	42	6.35	26	6.34	32	6.37	28	6.35	27
4.45	35	4.49	32	4.49	34	4.50	20	4.49	30
3.64	100	3.67	100	3.66	100	3.68	100	3.66	100
3.15	14	3.18	8	3.17	8	3.18	5	3.17	8
2.82	7	2.84	8	2.84	8	2.85	11	2.84	8
2.57	13	2.59	11	2.59	11	2.60	17	2.59	10
2.10	6	2.12	4	2.12	4	2.12	7	2.11	5
1.78	8	1.76	7	1.76	6	1.77	7	1.76	8

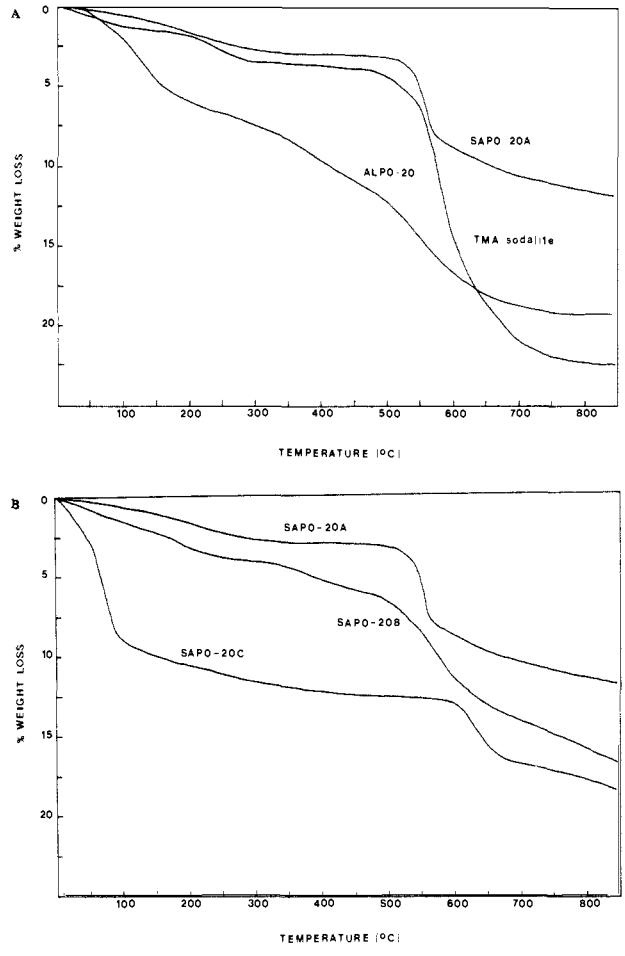

Figure 2. Thermogravimetric analyses: (A) $AlPO_4$-20, SAPO-20, TMA–sodalite; (B) SAPO-20A, SAPO-20B, SAPO-20C.

Thermal Decomposition Patterns. Figures 2 and 3 show the TGA and DTA results respectively for $AlPO_4$-20, SAPO-20, and sodalite. Sodalite, SAPO-20A, and SAPO-20C give two distinct weight losses: 25–300 and 500–700 °C. Each range has a characteristic pattern in the DTA. The first loss is due to the desorption of water. The second loss is accompanied by exotherms that indicate that they are from the decomposition of TMA. The decomposition patterns are distinctly different in each of these three materials, but they all begin above 500 °C. $AlPO_4$-20 and SAPO-20B give weight losses with associated exotherms below 500 °C. Interestingly, the DTA peaks at 400 °C for $AlPO_4$-20 and SAPO-20B align perfectly with the exotherm of pure $(TMA)OH{\cdot}5H_2O$ (see Figure 3).

^{13}C NMR Results. Figure 4 shows the cross-polarization ^{13}C NMR spectra for all five molecular sieves. The TMA within $AlPO_4$-20 gives a chemical shift of 57.67 ppm while TMA within sodalite yields 58.17 ppm. From the work of Baerlocher and Meier[13] it is known that in TMA–sodalite the TMA is balancing the negative framework. In $AlPO_4$-20, we believe that since the framework is neutral, TMA exists as (TMA)OH. Such is the case for tetrapropylammonium (TPA) in $AlPO_4$-5 synthesized with

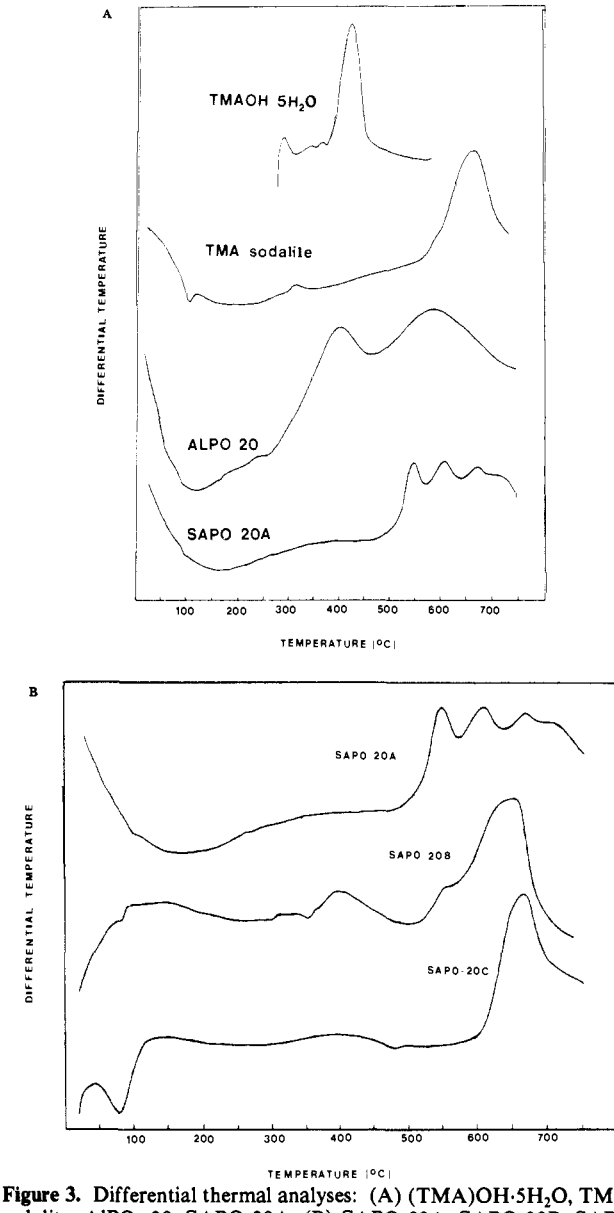

Figure 3. Differential thermal analyses: (A) $(TMA)OH{\cdot}5H_2O$, TMA–sodalite, $AlPO_4$-20, SAPO-20A; (B) SAPO-20A, SAPO-20B, SAPO-20C.

tetrapropylammonium hydroxide ((TPA)OH).[16] The fact that $AlPO_4$-20 gives a DTA exotherm at the same temperature as (TMA)OH also supports this conclusion. An upfield shift in the TMA resonance might be expected if TMA is balanced by OH rather than the framework since the value for (TMA)OH in D_2O (concentration dependent) is observed in the range 55.3–56.17 ppm (see Table IV). SAPO-20A gives two peaks, which are

(16) Bennett, J. M.; Cohen, F. P.; Flanigen, E. M.; Pluth, J. J.; Smith, J. V. *Intrazeolite Chemistry*; American Chemical Society: Washington, DC, 1983; pp 109–118.

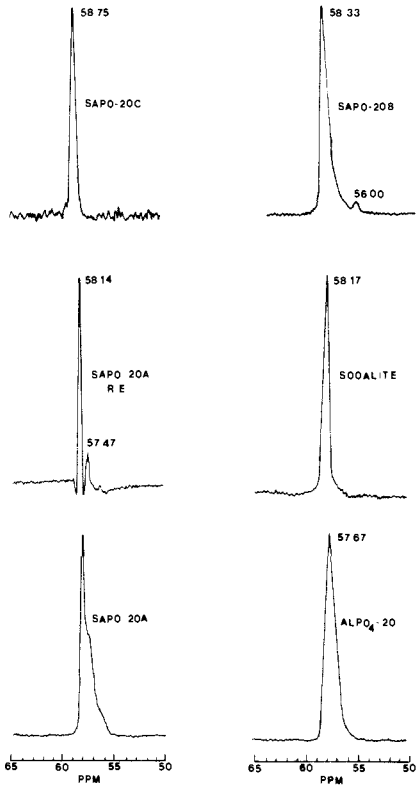

Figure 4. ^{13}C NMR spectra of molecular sieves.

Table IV. ^{13}C NMR Chemical Shift Data for TMA

sample	sites of TMA: β-cage	α-cage	surface	in D_2O	ref
ZK-4 (Si/Al = 1.16)	58.92				18
ZK-4 (Si/Al = 1.62)	58.84	56.94			18
ZK-4 (Si/Al = 2.71)	58.84	56.97			18
sodalite	58.84				18
TMA^+				56.4	18
Linde A	58.69	56.94	55.97		19
faujasite I	58.69	56.65			19
faujasite II			56.21		19
TMA^+				55.98–56.17	19
$AlPO_4$-20	57.67				this work
SAPO-20A	58.17, 57.44				this work
SAPO-20B	58.33		56.00		this work
SAPO-20C	58.75				this work
sodalite	58.17				this work
TMA^+				55.30	this work
SAPO-37	58.4				10

resolved with resolution enhancement (RE). Notice that these two resonances compare well with the resonances from sodalite and $AlPO_4$-20. SAPO-20B shows a large peak at 58.33 ppm with asymmetry on the upfield side and a small peak at 56.00 ppm. The small upfield peak (56 ppm) we tentatively assign to surface TMA (see Table IV, vide infra). Because of the upfield asymmetry, the large resonance is probably due to more than a single environment. SAPO-20C gives a single peak at 58.75 ppm, which is the farthest downfield of the five materials. Recall that this material contains sodium. We believe that all resonances in the range of 58–59 ppm are due to TMA cations, which balance negative charges of the framework. We speculate also that resonances around 57.5 ppm are due to (TMA)OH. Relaxation time experiments for proton and carbon are in progress.[17]

(17) Hasha, D.; Davis, M. E., to be submitted for publication.

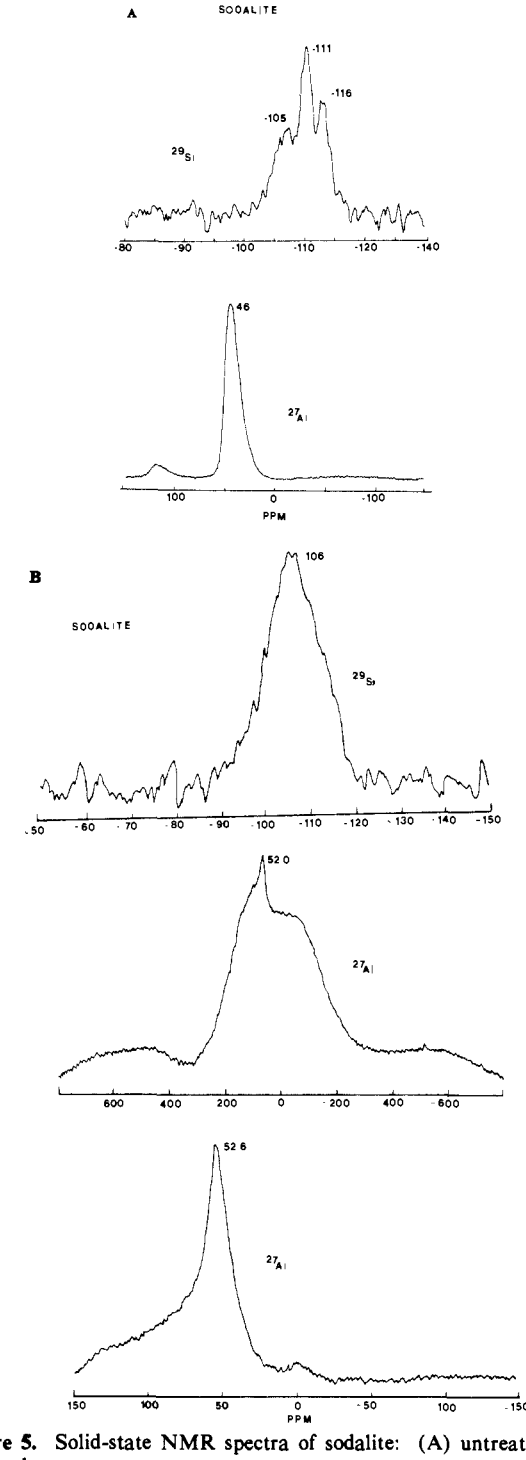

Figure 5. Solid-state NMR spectra of sodalite: (A) untreated, (B) calcined.

The ^{13}C chemical shift of TMA in zeolites correlates well with the size of the trapping cage.[18,19] In general, the larger the cage, the closer the chemical shift is to the value obtained from TMA in D_2O.[17] Also, Jarman and Melchior[18] report that the chemical shift of TMA does not vary with Si/Al for TMA in ZK-4. Table IV summarizes the chemical shift data for TMA in molecular sieves containing sodalite cages. Our results are in qualitative agreement with previous data. However, our chemical shifts show dependence upon the composition of the cage. This dependency is not as large as for changing cage type[19] but is real and must be considered when TMA is used to probe the cage structures of

(18) Jarman, R. H.; Melchior, M. T. *J. Chem. Soc., Chem. Commun.* **1984**, 414–416.
(19) Hayashi, S.; Suzuki, K.; Shin, S.; Hayamizu, K.; Yamamoto, O. *Chem. Phys. Lett.* **1985**, *113*, 368–371.

$AlPO_4$-*n* and SAPO-*n* molecular sieves.

^{29}Si, ^{27}Al, and ^{31}P NMR Results. Figure 5 shows the ^{29}Si and ^{27}Al NMR spectra for sodalite. The ^{29}Si spectrum for the as-synthesized sodalite gives three peaks (ppm) that have been assigned previously to the following: Si(2Al, 2Si),[20] −105; Si(1Al, 3Si), −111; Si(0Al, 4Si), −116.[21] The Si(0Al, 4Si) peak at −116 ppm is characteristic of the sodalite structure.[21] The signal-to-noise ratio in our ^{29}Si spectrum is not as large as reported by Jarman. Klinowski et al.[22] recently showed that the dominant source of the ^{29}Si spin–lattice relaxation in zeolites is paramagnetic oxygen molecules. Since sodalite-type structures cannot adsorb oxygen, this major relaxation mechanism is not available in these samples. In order to probe the possibility of low signal-to-noise ratios because of long relaxation times, we used delay times of 20 and 200 s and found the same results. Thus, the relaxation of ^{29}Si in our sample must be larger than 200 s. One possible explanation for the enhanced signal-to-noise ratio previously reported[21] could be the level of Fe^{3+} impurity. Iwamiya and Gerstein[23] indicated that the T_1 of ^{29}Si in offretite is dominated by dipolar coupling to a paramagnetic center in the framework and that this center may be some type of Fe^{3+} species. We did not analyze for Fe^{3+} in our samples.

The ^{27}Al NMR spectrum from the as-synthesized sodalite shows a single resonance at 46 ppm. We assign this chemical shift to Al(4Si). The small peak at 120 ppm is identified as a spinning sideband since it appears at different positions in spectra recorded at various spinning rates. Fyfe et al.[24] show that the chemical shift region for Al(4Si) in zeolites is approximately 50–65 ppm and report also a chemical shift of 61–65 ppm for sodalite. Our value is upfield from this region and is due to the presence of TMA (vide infra).

The ^{29}Si NMR spectrum of the calcined sodalite shows one broad peak centered at −106 ppm. Resolution of different silicon environments is not possible from this spectrum, but because of the chemical shift range, −90 to −115 ppm, the spectrum does indicate that several silicon environments are present.

Figure 5B shows the ^{27}Al NMR spectra for sodalite, which was calcined and partially dehydrated, and for the rehydrated material. For the partially dehydrated sample, a very broad signal is obtained along with a sharp resonance at 52.0 ppm. Upon hydration, the broadness disappears from the signal intensity, and a sharp peak at 52.6 ppm remains. The line broadening of the ^{27}Al NMR signal upon dehydration has been reported previously[25] and has been attributed to distortion in the aluminum tetrahedra. The chemical shift of the hydrated, calcined sample is downfield from the resonance obtained from the as-synthesized material. The chemical shift difference is most probably due to the change in cation from TMA^+ to H^+ upon calcination. The resonance at 52.6 ppm is now within the ^{27}Al chemical shift range for Al(4Si) reported previously.[24] However, this shift remains upfield from the values given by Fyfe et al.[24] The upfield shift is most probably because our sample contains no sodium and it possesses a higher Si/Al than those of Fyfe et al.

Figure 6 illustrates the ^{27}Al and ^{31}P NMR spectra for $AlPO_4$-20. The ^{27}Al and ^{31}P NMR spectra of the as-synthesized material both show two resonances. The chemical shifts of the two peaks in the ^{31}P spectrum indicate that the environments for phosphorus are P(4Al).[26] We suspect that one of the peaks could be due to the influence of the occluded organic. Upon calcination only one ^{31}P resonance is observed (see Figure 6B) at −35.2 ppm, indicating that our speculation is probably correct. The single resonance

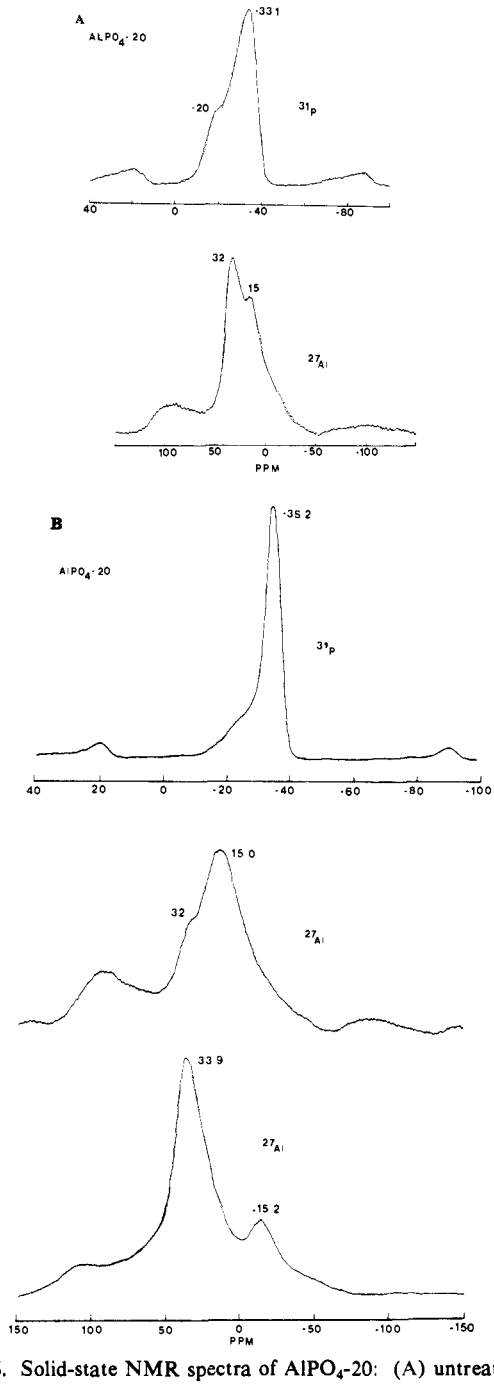

Figure 6. Solid-state NMR spectra of $AlPO_4$-20: (A) untreated, (B) calcined.

of −35.2 ppm is representative of P(4Al) in an aluminophoshate framework.[26] The chemical shifts for the two peaks in the ^{27}Al NMR spectrum of the as-synthesized material appear fairly close to those observed for SAPO-37.[10] Upon calcination and partial dehydration of $AlPO_4$-20, the ^{27}Al NMR spectrum changes. The relative intensities of the two peaks reverse, and the line widths increase slightly. After hydration of $AlPO_4$-20, the ^{27}Al NMR spectrum dramatically changes. The main resonance remains in the low 30 ppm chemical shift region, indicating Al(4P),[26] but the 15 ppm peak is replaced by a resonance at −15.2 ppm. These results are similar to those obtained by Blackwell and Patton[26] for $AlPO_4$-17. These authors suggest that the −15 ppm peak is not due to octahedral aluminum, i.e., extra framework, but rather to a secondary coordination of certain framework Al(4P) sites with strongly adsorbed water. This adsorbed water alters the aluminum environment sufficiently to produce an "octahedral" region chemical shift. In our previous work on SAPO-37,[10] we assigned this type of peak to extra-lattice aluminum. In retrospect, our assignment may not be justified in view of the data presented

(20) In the notation El_i (αEl_1, βEl_2, γEl_3), El_i (i = 1, 2, 3) denotes Si, Al, and P and α, β, and γ are the number of nearest neighbors that are bonded through bridging oxygen atoms. $\alpha + \beta + \gamma = 4$.

(21) Jarman, R. H. *J. Chem. Soc., Chem. Commun.* **1983**, 512–513.
(22) Klinowski, J.; Carpenter, T. A.; Thomas, J. M. *J. Chem. Soc., Chem. Commun.* **1986**, 956–958.
(23) Iwamiya, J. H.; Gerstein, B. C. *Zeolites* **1986**, *6*, 181–184.
(24) Fyfe, C. A.; Gobbi, G. C.; Hartman, J. S.; Klinowski, J.; Thomas, J. M. *J. Phys. Chem.* **1982**, *86*, 1247–1450.
(25) Kentgens, A. P. M.; Scholle, K. F. M. G. J.; Veeman, W. S. *J. Phys. Chem.* **1983**, *87*, 4357–4360.
(26) Blackwell, C. S.; Patton, R. L. *J. Phys. Chem.* **1984**, *88*, 6135–6139.

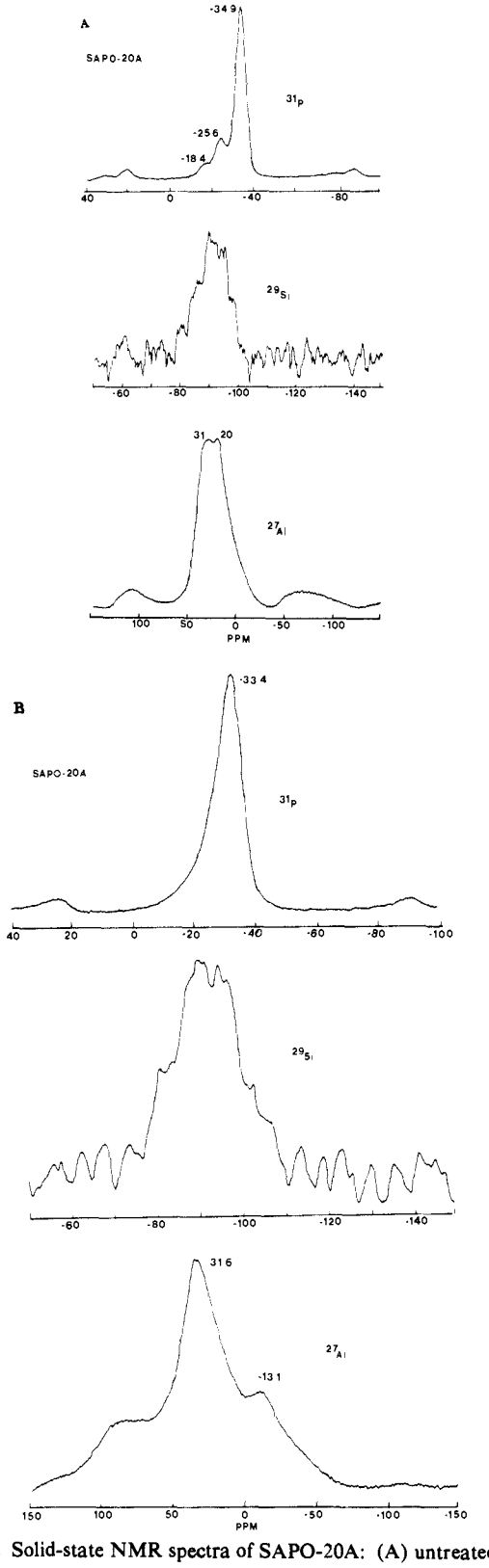

Figure 7. Solid-state NMR spectra of SAPO-20A: (A) untreated, (B) calcined.

here (vide infra). Most probably, the −15 ppm environment is described properly by Blackwell and Patton. This point is discussed further below.

Figure 7 shows the ^{29}Si, ^{27}Al, and ^{31}P NMR spectra for SAPO-20A. The ^{29}Si NMR spectra before and after calcination remain fairly constant. There are no distinct peaks within the broad envelope of signal intensity, but the fact that the intensity spans such a large chemical shift range indicates that there are several environments for silicon in SAPO-20A. These data imply that a single substitution mechanism must not be occurring. In our previous work on SAPO-37,[10] we clearly showed that silicon substitutes for phosphorus only (mechanism 2) and that the ^{29}Si NMR spectrum contained only a single well-resolved resonance at −90.21 ppm. The chemical shift range spanned by the ^{29}Si NMR spectra in Figure 7 implies that Si–O–Si linkages must be present. Therefore, we believe that substitution mechanisms 2 and 3 are occurring. It is interesting to note that if a 1/1 ratio of mechanisms 2 and 3 is used, the exact chemical composition is obtained. Mechanism 2 must be occurring because this material shows the presence of hydroxyl groups upon air calcination (vide infra).

The ^{27}Al and ^{31}P NMR spectra for SAPO-20A are fairly similar to those obtained from $AlPO_4$-20. Notice that the ^{31}P spectrum contains several resonances before calcination. After calcination, a single peak appears around −35 ppm, indicating P(4Al). The ^{27}Al NMR spectrum before calcination reveals two peaks in equal intensity at 31 and 20 ppm. Upon calcination and partial dehydration (not shown), the ^{27}Al spectrum again resembles the $AlPO_4$-20 spectrum in that the intensity of the 31 ppm peak is lower than the intensity of the 20 ppm resonance. After hydration, two peaks appear at 31.6 and −13.1 ppm. The band downfield from the 31.6 ppm peak is a spinning sideband.

Since it is clear that silicon resides in several environments in SAPO-20A and the framework does contain negative charges, more than a single substitution mechanism must be taking place. Obviously, mechanism 2 occurs because it is the only one that gives rise to negative framework charges. Silicon substitution by this mechanism implies that there be Si(4Al) sites that are characterized by a ^{29}Si chemical shift near −90 ppm.[10] Substitution mechanism 1 leads to Si(4P) environments and positive framework charges. To date, there is no evidence for positive framework charges in SAPO-*n* materials. Also, the Si(4P) environment is highly unlikely. It is more probable that if silicon is surrounded by phosphorus, it will be octahedral rather than tetrahedral on the basis of known silicon–phosphorus compounds.[27,28] Thus, no chemical shift data are available for tetrahedral silicon with phosphorus neighbors. However, the ^{31}P chemical shifts for SiP_2O_7 range from −46 to −54 ppm.[28] The influence of the octahedral silicon on the ^{31}P chemical shift gives rise to values upfield from the ^{31}P chemical shift region of aluminophosphates. Since the ^{31}P chemical shift obtained from SAPO-20A is not upfield from the $AlPO_4$-20 chemical shift, we rule out substitution mechanism 1. Finally, we address substitution mechanism 3. If one views mechanism 3 as the substitution of an aluminum–phosphorus pair by a silicon pair in an aluminophosphate structure, then this substitution would give silicon environments of Si(1Si, 3Al) and Si(1Si, 3P). The latter environment is highly unlikely for reasons outlined previously. It is correct to view the substitution mechanisms in terms of rationalizing the bulk composition as originally stated by Lok et al.[4b] However, one must be careful in stretching the interpretation further. Mechanism 3 implies substitutions that do not create framework charge via substitution by silicon pairs. We believe silicon pairs can be formed in SAPO-*n* structures because of the ^{29}Si NMR data for SAPO-20A, which show multiple silicon environments. However, since the chemical shifts are for silicon surrounded by silicon and aluminum, the silicon environments must be Si(xSi, $(4-x)$Al), where $x = 1$–4, rather than Si(1Si, 3Al) and Si(1Si, 3P). If such is the case, then the aluminum environments are Al(1Si, 3P) and Al(4P). We cannot rule out the possibility of both environments. The Al(1Si, 3P) environment must exist because of the results given by the ^{29}Si and ^{31}P NMR spectra. This environment was observed in SAPO-37.[10] Since there are not two resonances in the tetrahedral region of the ^{27}Al NMR spectrum for calcined, hydrated SAPO-20A, either the Al(4P) environment does not exist or it cannot be distinguished from the Al(1Si, 3P) environment on the basis of chemical shift (see ^{27}Al NMR spectrum of $AlPO_4$-20). Thus, the combined ^{29}Si, ^{27}Al, and ^{31}P NMR spectra are consistent

(27) Hesse, K. F. *Acta. Crystallogr., Sect. B: Struct. Crystallogr. Cryst. Chem.* **1979**, *B35*, 724–725.
(28) Mudrakovskii, I. L.; Mastikhin, V. M.; Shmachkova, V. P.; Kotsarenko, N. S. *Chem. Phys. Lett.* **1985**, *120*, 424–426.

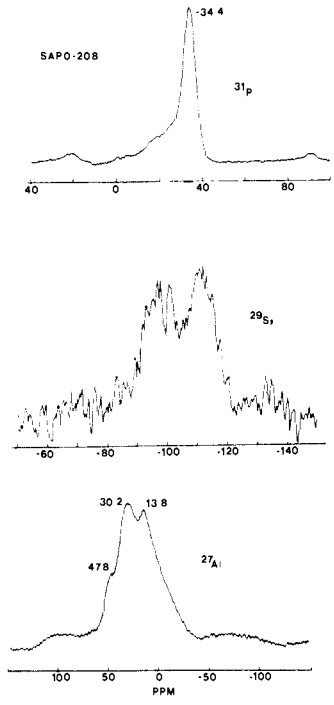

Figure 8. Solid-state NMR spectra of SAPO-20B.

with silicon substitutions on the basis of mechanisms 2 and 3. These combined substitutions could lead to regions in the solid where the framework is neutral and regions where it is anionic. This could be the reason for observing two ^{13}C environments for TMA; one for TMA^+ and the other for (TMA)OH (see Figure 4).

SAPO-20B contains a larger atom fraction of silicon than SAPO-20A (see Table II). The ^{29}Si, ^{27}Al, and ^{31}P NMR spectra for SAPO-20B are illustrated in Figure 8. Notice that the ^{31}P spectrum resembles that observed from $AlPO_4$-20 and SAPO-20A after calcination while the ^{27}Al and ^{29}Si spectra are different. The ^{27}Al NMR spectrum appears like those for $AlPO_4$-20 and SAPO-20A with the addition of a resonance at 47.8 ppm. Likewise, the ^{29}Si NMR spectrum resembles that of SAPO-20A except for the increased intensity around −115 ppm. Recall that an ^{27}Al resonance at a chemical shift around 46–47 ppm is for Al(4Si), and a ^{29}Si shift at −116 ppm is characteristic of Si(4Si) in the sodalite structure (refer to Figure 5). Therefore, we conclude that SAPO-20B is similar to SAPO-20A except that it includes regions that are "sodalite-like". It is interesting to note that we could not detect these regions by electron microprobe analysis (spot size ~1 μm). Given a sufficiently high resolution microprobe, we believe that these regions will become apparent. Because SAPO-20B is not homogeneous, we did not calcine the sample for further NMR experiments. It is surprising that SAPO-20B did not show several distinct ^{13}C environments like SAPO-20A. However, it is possible that the upfield asymmetry could be due to additional ^{13}C environments.

Figure 9 shows the ^{29}Si, ^{27}Al, and ^{31}P NMR spectra for SAPO-20C. The ^{29}Si spectra again reveal that silicon is residing in several environments of the type Si(xSi, $(4-x)$Al), where x = 1–4. However, notice that the signal intensity as a whole is downfield from that observed from sodalite, indicating more aluminum-rich environments in SAPO-20C. This is expected from the chemical compositions of SAPO-20C and sodalite (see Table II). The ^{31}P NMR spectrum of the as-synthesized materials shows three peaks. The main resonance at −31.4 ppm is indicative of P(4Al). Thus, phosphorus is in a tetrahedral site in the framework. Phosphorus incorporation into zeolite frameworks was first reported by Flanigen and Grose.[29] Since that time, there has been

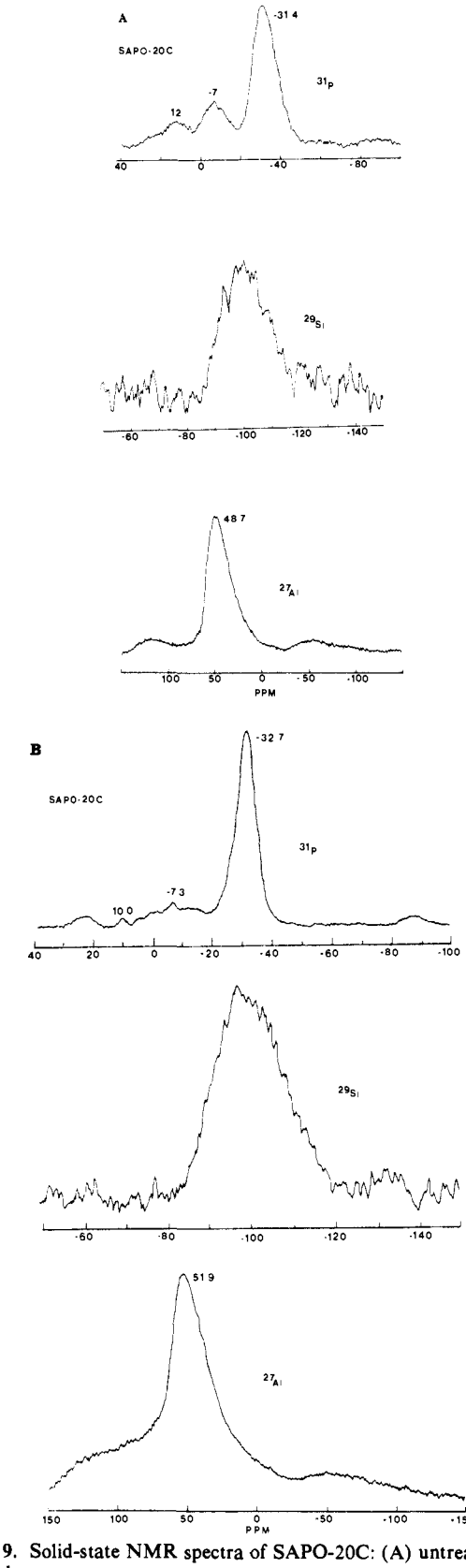

Figure 9. Solid-state NMR spectra of SAPO-20C: (A) untreated, (B) calcined.

some controversy[30] over this claim. We show here strong support for the claims of Flanigen and Grose. The resonances at 12 and −7 ppm are most probably due to occluded phosphate, which is balanced by Na^+ and TMA^+. Upon calcination these peaks

(29) Flanigen, E. M.; Grose, R. W. *Molecular Sieve Zeolites-I*; Gould, R. F., Ed.; Advances in Chemistry 101; American Chemical Society: Washington, DC, 1971; p 76.

(30) Barrer, R. M. *Hydrothermal Chemistry of Zeolites*; Academic: London, 1982; p 294.

Table V. XPS Data for Molecular Sieves

sample	superficial region oxide composition	binding energy,[a] eV			
		Si, 2P	Al, 2P	P, 2P	O, 1s
$AlPO_4$-20	$(Al_{0.52}P_{0.48})O_{2.2}$		75.3	134.8	532.7
SAPO-20A	$(Al_{0.55}Si_{0.10}P_{0.35})O_{2.2}$	101.6	75.0	134.7	532.6
SAPO-20B	$(Al_{0.35}Si_{0.48}P_{0.16})O_{2.2}$	102.7	74.8	134.9	532.8
SAPO-20C	$(Al_{0.44}Si_{0.41}P_{0.15})O_{2.1}$	102.1	74.4	134.6	532.0
sodalite	$(Al_{0.2}Si_{0.8})O_{2.2}$	103.0	74.2		532.7
SAPO-37[b]	$(Al_{0.54}Si_{0.13}P_{0.33})O_{2.3}$	101.9	74.4	134.2	531.8
$AlPO_4$-5 ($Al_{0.5}P_{0.9}$)[c]	$(Al_{0.52}P_{0.48})$		75.2	134.6	532.3
$AlPO_4$-11 ($Al_{0.5}P_{0.9}$)[c]	$(Al_{0.57}P_{0.43})$		75.3	134.8	532.4
SAPO-5 ($Al_{0.41}Si_{0.20}P_{0.39}$)[c]	$(Al_{0.51}Si_{0.20}P_{0.20})$	102.7	75.0	134.5	531.9
NaA[c]		101.5	73.6		530.8
NaX[c]		101.7	73.8		530.7
NaY[c]		102.7	74.3		531.7
ZSM-5[c]		103.1	73.9		532.4

[a] Reference for samples from this work is the Au $4f_{7/2}$ transition at 83.8 eV. [b] Same material used in ref 10. [c] From ref 31. Composition in parentheses is the bulk composition. Binding energies referenced to C 1s at 284.6 eV.

decrease in magnitude. The balancing cations after calcination must be Na^+ and H^+. The ^{27}Al spectra show one peak before and after calcination, similar to that obtained from sodalite. However, the peaks from SAPO-20C reveal asymmetry on the upfield side. The ^{27}Al NMR spectra of partially dehydrated SAPO-20C resemble the behavior illustrated by sodalite rather than $AlPO_4$-20 or SAPO-20A. We assign the ^{27}Al resonance for SAPO-20C to Al(3Si, 1P) and Al(4Si) environments. The Al(3Si, 1P) environment is novel and is justified further below. Since phosphorus is P(4Al), at least a portion of the aluminum atoms must have phosphorus neighbors. We make the assignment of one P neighbor on the basis of the chemical shift. If more P neighbors surrounded Al, then the ^{27}Al chemical shift should be further upfield (aluminophosphate region). The aluminum environment in SAPO-20C is different from that in sodalite, $AlPO_4$-20, SAPO-20A, and SAPO-20B as evidenced by its binding energy measured by XPS (vide infra). It is interesting to note that the ^{27}Al NMR spectra of Al(4P) and Al(1Si, 3P) appear not to be distinguishable by chemical shift differences, and we now propose that the same is true for Al(4Si) and Al(3Si, 1P). Also, the silicon-rich and phosphorus-rich environments at aluminum show two distinct behaviors with dehydration and rehydration. The silicon-rich environments do not reveal an octahedral region chemical shift upon hydration.

At this time, the substitution mechanisms that are occurring in SAPO-20C are unclear. Most probably, P^{5+} is substituting for Si^{4+} and/or an Al^{3+}, P^{5+} pair is replacing $2Si^{4+}$. It is expected that Na^+ and TMA^+ balance the anionic framework, and upon calcination acid sites are formed (vide infra). The ^{13}C chemical shift of TMA is approximately 0.5 ppm downfield from the value obtained for TMA–sodalite and is similar to values for zeolite A, faujasite, and sodalite, all of which contain sodium (see Table IV). Therefore, the TMA in SAPO-20C is assigned to TMA^+ balancing anionic framework sites, and the downfield shift relative to TMA–sodalite is most probably due to the influence of sodium.

All of the above data lead to the conclusion that in SAPO-*n* molecular sieves Si–O–P linkages are not observed. Silicon atoms are found to have silicon and/or aluminum neighbors while phosphorus is surrounded by aluminum only. Two distinct physicochemical environments of aluminum are observed: phosphorus rich and silicon rich. Thus, in terms of substitution mechanisms, Si^{4+} can substitute for P^{5+} and vice versa, and Si–O–Si can substitute for Al–O–P and vice versa.

XPS Results. Table V shows the oxide composition of the superficial region of each molecular sieve and the binding energies of the framework atoms. Data from Suib et al.[31] are included also in Table V for comparison. Notice that the superficial and bulk oxide compositions of $AlPO_4$-20, SAPO-20A, and sodalite are fairly similar while those of SAPO-20B and SAPO-20C are different. The major change in the oxide composition of the latter two materials is the Si/Al; the superficial region appears aluminum rich for SAPO-20C and silicon rich for SAPO-20B. Zoning of aluminum in ZSM-5 is well-known[32] and may be occurring in SAPO-20B and SAPO-20C.

The binding energy of the phosphorus 2p transition is the same to within experimental error for the molecular sieves with the sodalite structure. Also, the 134.7 ± 0.2 eV binding energy is consistent with those reported for other SAPO and $AlPO_4$ molecular sieves.[31] Recall that the ^{31}P chemical shift is essentially the same for $AlPO_4$ and SAPO materials, and that leads us to assign phosphorus to P(4Al) in the SAPO molecular sieves. Since the binding energy of phosphorus is the same in $AlPO_4$ and SAPO materials, the XPS data support the conclusions concerning the phosphorus environment in the SAPO molcular sieves.

The oxygen 1s transition shows a consistent binding energy for the sodalite-type molecular sieves except SAPO-20C. SAPO-20C is the only solid in this series of materials that contains sodium. Notice that for NaA, NaX, and NaY (high Na^+ content) the oxygen 1s binding energy is lower than that reported for ZSM-5 (low Na^+ content) and the molecular sieves (no Na^+). Thus, we believe the lower binding energy for oxygen 1s in SAPO-20C is due to the presence of sodium.

The binding energy of the silicon 2p transition shows increases with the number of silicon neighbors in the zeolites. Notice that the binding energy increases as Si/Al gets larger (Si/Al: NaA < NaX < NaY < ZSM-5). In SAPO-37, we showed the silicon is in the single environment Si(4Al).[10] The environments of silicon postulated from the NMR results (vide supra) give this same trend for silicon. Again, the XPS data are consistent with our NMR assignments.

The binding energy of the aluminum 2p transition decreases with increasing silicon content of the molecular sieve. Notice the decline in the binding energy when going from $AlPO_4$-20 to sodalite. There is a clear difference in binding energies between the group $AlPO_4$-20, SAPO-20A, and SAPO-20B and the pair SAPO-20C and sodalite. Recall that these are exactly the two groups that are distinguished by the ^{27}Al NMR chemical shift and also the ^{27}Al NMR characteristics upon dehydration/hydration. The silicon-rich environments (sodalite, SAPO-20C) give lower aluminum 2p binding energies than the phosphorus-rich ones ($AlPO_4$-20, SAPO-20A, SAPO-20B). Notice that there is a distinguishable difference (several repeat experiments performed) in the binding energy for $AlPO_4$-20 and SAPO-20A where we have postulated the environments to be Al(4P) and Al(4P) and/or Al(3P, 1Si), respectively. Also, SAPO-20C (Al(4Si) and/or Al(3Si, 1P)) and sodalite (Si(4Al)) show a difference in the aluminum 2p binding energy. These XPS data support further our assignments of the solid-state NMR resonances.

(31) Suib, S. L.; Winicki, A. M.; Kostapapas, A. *Langmuir* **1987**, *3*, 483–488.

(32) von Ballmoos, R.; Gubser, R.; Meier, W. M. *Proceedings of the Sixth International Zeolite Conference*; Olson, D., Bisio, A., Eds.; Butterworths: Guildford, England, 1984; p 803.

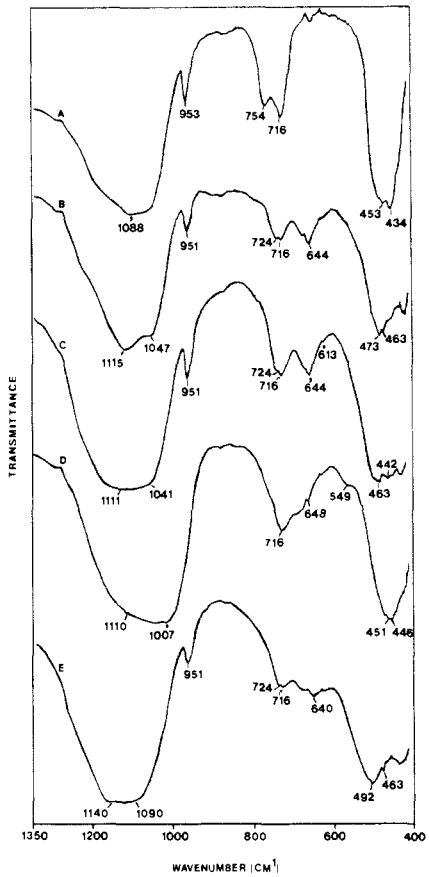

Figure 10. Infrared spectra of the structural region for molecular sieves: (A) sodalite, (B) SAPO-20A, (C) SAPO-20B, (D) SAPO-20C, (E) $AlPO_4$-20.

Infrared Results. Figure 10 shows the infrared spectra of the structural region for the five molecular sieves with the sodalite structure. The infrared spectrum of TMA–sodalite is illustrated by A. The peak at 953 cm^{-1} is from TMA^+. Flanigen et al.[33] show the infrared spectrum for hydroxy sodalite. In general spectrum A agrees with that of Flanigen et al. except that the absorptions between 700 and 760 cm^{-1} are at higher wavenumber (754 and 716 cm^{-1} compared to 729 and 660 cm^{-1}). The broad band around 1000–1100 cm^{-1} has been assigned to the asymmetric stretching of tetrahedra[33] and is characteristic of zeolite materials. Notice that, for SAPO-20A, SAPO-20B, and $AlPO_4$-20, this region is shifted to higher wavenumber. The shift is due to the presence of large amounts of phosphorus since the P–O bond distance is shorter than either Si–O or Al–O. SAPO-20C shows a very broad absorption in this region as might be expected since the solid contains some phosphorus but still possesses a Si/Al of a zeolite. In the region of 750 cm^{-1} and below, there are many differences in the number and frequency of the absorptions for the five materials reflecting the variation in framework composition.

Finally, upon calcination of SAPO-20A, SAPO-20B, and SAPO-20C, hydroxyl group absorptions are observed for each material. Thus, at least a portion of the TMA in all three samples is compensating framework charge.

Conclusions

The overall results of this study and our previous work[10] lead to the following conclusions. The atomic arrangements of Al, Si, and P in molecular sieves are such that Si–O–P linkages are not observed. Thus, in terms of substitution mechanisms, Si^{4+} can substitute for P^{5+} and vice versa, and Si–O–Si can substitute for Al–O–P and vice versa.

Acknowledgment. Financial support of this work was provided by the National Science Foundation under the Presidential Young Investigator Award to M.E.D. and The Dow Chemical Co. We thank Dr. Steven Suib, Chemistry Department, University of Connecticut, for the XPS analysis of SAPO-37.

Registry No. (TPA)OH, 4499-86-9; (TMA)OH, 75-59-2; $(TMA)^+$, 51-92-3; Cab-O-Sil, 7631-86-9; H_3PO_4, 7664-38-2; Al(O)(OH), 24623-77-6.

(33) Flanigen, E. M.; Khatami, H.; Szymanski, H. A. *Molecular Sieve Zeolites-I*; American Chemical Society: Washington, DC 1971; p 201–228.

The System Pyridine–Hydrogen Fluoride at Low Temperatures: Formation and Crystal Structures of Solid Complexes with Very Strong NHF and FHF Hydrogen Bonding[1,2]

Dagmar Boenigk and Dietrich Mootz*

Contribution from the Institut für Anorganische Chemie und Strukturchemie, Universität Düsseldorf, D-4000 Düsseldorf, Federal Republic of Germany. *Received August 10, 1987*

Abstract: The formation of solid complexes at low temperatures in the system pyridine–hydrogen fluoride was studied by difference thermal analysis and X-ray powder diffraction. The melting diagram obtained reveals the existence of as many as eight intermediary compounds $C_5H_5N{\cdot}nHF$ with melting points between −1 and −124 °C and n assuming all integral values from one to eight. The crystal structures of four of these were determined from single-crystal Mo Kα diffractometer data: $C_5H_5N{\cdot}1HF$ (crystal system tetragonal, space group $P4_12_12$, $Z = 4$ formula units per unit cell), $C_5H_5N{\cdot}2HF$ (monoclinic, $P2_1/m$, $Z = 2$), $C_5H_5N{\cdot}3HF$ (triclinic, $P\bar{1}$, $Z = 2$), and $C_5H_5N{\cdot}4HF$ (monoclinic, $P2_1/m$, $Z = 2$). In the complex with $n = 1$ the base is not protonated by the acid and furnishes the first observation of the hydrogen bond F–H···N by crystal structure analysis. With an F···N distance of 247.2 (2) pm it is the strongest one known between a fluorine and a nitrogen atom. The remaining structures contain pyridinium cations and complex $H_{n-1}F_n^-$ anions and are governed by hydrogen bonding, too, between the cations and anions (N–H···F) as well as within the anions (F–H···F). Coulombic interaction appears to be largely internalized in discrete ionic pairs ($n = 2$ and 3) and a one-dimensional ribbon structure ($n = 4$).

The system pyridine–hydrogen fluoride is of practical importance in preparative organic chemistry. A solution in the pure base of about 70 wt % of anhydrous hydrogen fluoride (equivalent to 90 mol %) is described,[3] and in wide use, as a convenient reagent

0002-7863/88/1510-2135$01.50/0